

Article

Kinematic Analysis and Motion Planning of Cable-Driven Rehabilitation Robots

Jingyu Zhang , Dianguo Cao  and Yuqiang Wu *

School of Engineering, Qufu Normal University, Rizhao 276826, China; zhangjingyuwang@163.com (J.Z.); caodg@qfnu.edu.cn (D.C.)

* Correspondence: wyq@qfnu.edu.cn; Tel.: +86-1876-933-2022

Abstract: In this study, a new cable-driven rehabilitation robot is designed, the overall design of the robot is given, and the kinematic equation of the lower limbs in the supine state of the human body is addressed. Considering that cable winders move along the rail brackets, the closed vector method is applied to establish the kinematic model of the robot, and the relationship between the human joint angle and the cable length change was deduced. Considering joint compliance, a fifth-order polynomial trajectory planning method based on an S-shaped curve is proposed by introducing an S-shaped velocity curve, and the changes in cable length displacement, velocity, and acceleration are simulated and analyzed. Three planning methods are compared based on two indices, and experimental verification is carried out on the rehabilitation experiment platform. The simulation and experimental results show that the trajectory planning method presents low energy consumption and strong flexibility, and can achieve better rehabilitation effect, which builds a good basis for the subsequent study of dynamics and control strategy.

Keywords: cable-driven rehabilitation robot; kinematics; trajectory planning; fifth-order polynomial; flexibility



Citation: Zhang, J.; Cao, D.; Wu, Y. Kinematic Analysis and Motion Planning of Cable-Driven Rehabilitation Robots. *Appl. Sci.* **2021**, *11*, 10441. <https://doi.org/10.3390/app112110441>

Academic Editor: Dario Richiedi

Received: 23 September 2021

Accepted: 3 November 2021

Published: 6 November 2021

Publisher's Note: MDPI stays neutral with regard to jurisdictional claims in published maps and institutional affiliations.



Copyright: © 2021 by the authors. Licensee MDPI, Basel, Switzerland. This article is an open access article distributed under the terms and conditions of the Creative Commons Attribution (CC BY) license (<https://creativecommons.org/licenses/by/4.0/>).

1. Introduction

With the number of patients with limb injuries caused by unknown diseases or unexpected accidents increasing year by year [1,2], scientific and effective rehabilitation therapy plays a significant role in restoring limb motor function. In the early stage of rehabilitation, meaningful and repetitive rehabilitation training tasks can help patients with motor dysfunction improve their muscle strength and coordination [3,4]. Traditional rehabilitation treatment requires rehabilitation training under the guidance of rehabilitation specialists. Due to long-term training, the rehabilitation teacher's strength is weakened and the movement is biased, which leads to a weakening of the rehabilitation effect. For repetitive rehabilitation treatment, rehabilitation robots can be used instead of rehabilitation specialists [5]. Therefore, rehabilitation robots have received great attention.

Some exoskeleton rehabilitation robots have been widely applied in rehabilitation treatment, and help patients complete rehabilitation training more effectively through auxiliary training and real-time status monitoring [6], such as ARMin [7], RUPERT [8], and CADEN-7 [9]. However, the traditional exoskeleton robot has large inertia, and the patient is prone to collide with the robot, causing secondary injury to the patient. There are problems such as limited working space and a single training mode [10–12]. For these reasons, in recent years, cable-driven robots have begun to attract people's attention. They use cables to replace rigid elements to drive limb movement. They have the characteristics of a large working space, lower motion inertia, strong load-bearing capacity, and good flexibility [13–15] in multiple scenarios, they can satisfy the rehabilitation needs of different patients. In addition, when the robot is not controlled, the flexible cable can ensure that the patient is not injured. Therefore, cable-driven rehabilitation robots have been widely used in rehabilitation training. Ming et al. [16] developed a new type of cable-driven sports training

system. People need to train on a treadmill, and the traction cable can provide resistance to the legs and effectively improve the movement function of the legs. Wang et al. [17] designed the rehabilitation system that introduces a rigid chain, and experimental research is conducted on the training trajectory of the lower limb traction point in accordance with the planning strategy of rigid body movement. Ennaiem et al. [18] designed a three-degree-of-freedom planar cable-driven robot, which selects single objective optimization to help patients better complete the specified actions of upper limbs. Yang et al. [19] designed a rehabilitation robot combining a cable-driven mobile platform and an adjustable lower extremity exoskeleton device, which can perform rehabilitation training on the waist and lower limbs. Wang et al. [20] developed rigid-flexible hybrid lower limb rehabilitation robot comprehensively considers the cable tension, position of the traction points and system stiffness to study its dynamic stability evaluation method, which provides a consultation for rehabilitation training task planning and control strategies. Rogério et al. [21] developed a cable-driven parallel rehabilitation robot for basic movements of the lower limbs. The system consists of a fixed base and a mobile platform that can connect up to six cables. Wang et al. [22] designed a rehabilitation robot that can realize adduction and abduction of lower limbs, and the relationship of human-machine coordinated motion is considered. Kim et al. [23] developed a four-cable traction lower-limb rehabilitation robot for auxiliary training of gait, and the kinematics of the robot was optimized.

To improve the adaptability of cable-driven robots, the reconfigurable robots are proposed. Rosati et al. [24] designed an adaptive cable-drive system that modifies the pulley arrangement based on the pose of the end-effector to maintain optimal performance. Nguyen et al. [25] designed a reconfigurable suspended cable-driven robot for aircraft maintenance and obtained the optimal configuration of the robot by solving a multi-objective optimization problem. Gagliardini et al. [26] designed a discrete reconfigurable planning method for an 8-6 cable-driven robot that uses Dijkstra's algorithm to select the best reconfiguration strategy. There is also some research on the configurable aspects of cable-driven rehabilitation robots. MariBot is a 5-degree-of-freedom serial-parallel robot, two rotational joints of serial structure provide a wide horizontal range of upper limb movement [27]. Mao et al. [28] designed the cable-driven exoskeleton robot; they optimized the positions of the cable connection points by using the deviation area between the actual and desired trajectory of the robot arm as the optimization objective. Sophia-3 is an adaptive cable-driven device with a tilting working plane, which can achieve excellent force capabilities with fewer cables by moving the pulley lock [29].

Through the comprehensive analysis of the above research, it is found that the proposed cable-driven rehabilitation robots do not consider the compliance of rehabilitation trajectory from the perspective of human joints, and the designed cable exit points only move in a single direction. For these reasons, according to the tasks and characteristics of rehabilitation, this study comprehensively considers the angle flexibility of human joints and the configurability of cable exit points. A new trajectory planning method is proposed, which is used to improve joint flexibility. The cable exit points can move in two directions, and the cable exit points can rotate according to the direction of the cable, which effectively improves the workspace. Compliant action can improve the patient's comfort and promote early recovery; therefore, it is very important to plan the rehabilitation trajectory reasonably during the rehabilitation training process. In the early stage of rehabilitation, robots need to provide auxiliary motion suitable for human rehabilitation on the basis of the characteristics of human body structure. Therefore, kinematic analysis and trajectory planning simulation of the robot need to be carried out in advance [30]. The model of a cable-traction lower limb is similar to a multilink cable-driven manipulator. Rezazadeh et al. [31] proposed a systematic method for determining the tensionable workspace of a multibody cable-drive mechanism, the method is applied to several single-degree-of-freedom and two-degree-of-freedom mechanisms with different cable distributions. Lau et al. [32] proposed a generalized model of a multilink cable-driven serial manipulator and derived the kinematics and dynamics of the generalized model based on the cable-routing matrix. In

this study, a new type of cable-driven rehabilitation robot is conceived. Its cable exit point can move on the rail brackets in two directions and can provide rehabilitation training of various postures. To achieve a better rehabilitation effect, the relationship between the change in the human joint angle and the change in cable length is analyzed, and a new trajectory planning method is presented. Simulation and experiments verify the effectiveness and feasibility of this method.

2. Structure of Rehabilitation Robot and Human Lower Limb Model

2.1. Structure of Robot

The overall design of the cable-driven rehabilitation robot is shown in Figure 1a. The design mainly includes 4 columns, 5 rail brackets, 2 crossbeams, 6 synchronous belts, 8 servo motors ($S1-S8$), 6 DC motors, and 6 cable winders ($A1-A6$). As shown in Figure 1b, each rail bracket is equipped with a synchronous belt with a cable winder (two cable winders are installed on the middle rail brackets, and only one cable is shown in the Figure 1a), and each cable winder is equipped with an encoder, which is directly connected to the pulley. The DC motors and cable winders are assembled together, and the DC motors are used to drive the cable winders to realize the retraction and release of the cables. The cable will make the pulley turn, therefore, the encoder can directly measure the cable length. The connection of the cable winders with the rail brackets is rotatable, the exit point of the cable can be automatically adjusted according to the direction of the cables. The servo motors drive the synchronous belt to move the cable winders on the rail brackets. In addition, servo motors $S3$ and $S7$ also move the rail brackets on both sides up and down along the columns, and $S8$ allows the middle rail bracket to move left and right along the crossbeams. Therefore, while moving along the rail brackets, the cable winders $A4$ and $A5$ can move up and down, $A1$ and $A6$ can move left and right, which effectively improves the workspace of rehabilitation. The cable winders do not directly contact the limb, but indirectly control limb movement by monitoring the cables. One end of the cable is connected to the drum of the cable winder, and the other end is connected to the patient's limbs through a flexible belt. On the one hand, it can detect cable tension; on the other hand, it can play a buffering role, which improves the safety of rehabilitation training. The rehabilitation robot can provide multi-posture rehabilitation training, and can freely choose horizontal, sitting, vertical, and other training postures according to different rehabilitation states of the body and joint adaptation. The movement of the cable winders and the retraction and release of the cables is controlled by selecting different rehabilitation actions and the number of cables. Consequently, the patient's limbs can move in three-dimensional space and adjust in accordance with the changes of the interaction between the limbs and the rehabilitation robot to complete the rehabilitation treatment action in real time.

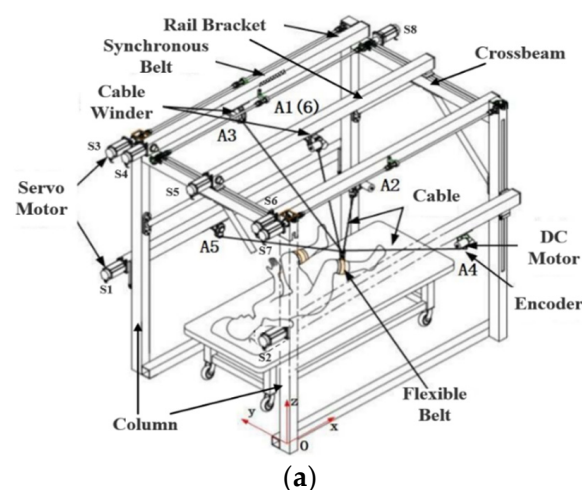


Figure 1. Cont.

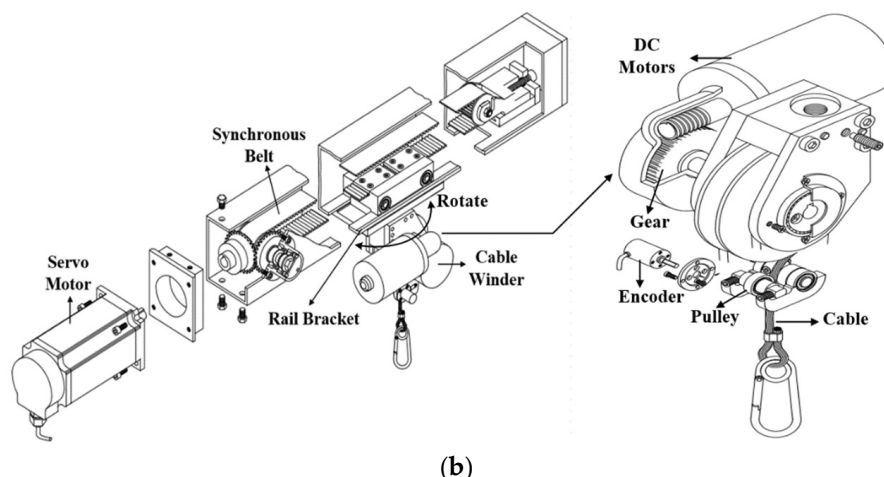


Figure 1. (a) Overall design of cable-driven rehabilitation robot. (b) Schematic diagram of the mechanism of DC motor and servo motor.

2.2. Human Lower Limb Model

During rehabilitation training, the patient’s body is in a horizontal posture of pitching, and the hip joints of the lower limbs are fixed in the middle of the bed. Considering the movement of the lower limbs, the structure of the lower limbs is analyzed, and a coordinate system in the lower limbs of the human body is established [33], as shown in Figure 2. $O - xyz$ is the global coordinate system, O_0 is the hip position, which is used as the base reference system $O_0 - x_0y_0z_0$, O_p is the position of the end ankle and is fixedly connected to the end ankle. The zero connecting rod is used to adjust the height of the hip joint and without causing rotation. The intersection of joint 1, joint 2, and joint 3 intersect at one point, which is the hip joint; joint 4 and joint 5 intersect at one point, which is the knee joint; and joint 6 is the ankle joint, its rotation will not affect the end trajectory; d_1 is the length of the thigh; and L_2 is the length of the lower leg. Table 1 shows the Denavit–Hartenberg (D–H) parameter, and the comfortable range of motion of the human hip joint is determined according to the maximum range of motion of the human hip joint [34]. In light of the principle of kinematics [35,36], the transformation matrix of the lower limb p_oT is

$${}^p_oT = \begin{bmatrix} R_{3 \times 3} & P_{3 \times 1} \\ 0 & 1 \end{bmatrix} \tag{1}$$

where $R_{3 \times 3}$ is the rotation matrix and $P_{3 \times 1}$ is the spatial position, which represents the orientation and position of the end ankle relative to the base reference coordinate system, respectively. The posture changes of the end ankle can be obtained by reasonably planning the angles of each joint. In the process of rehabilitation, the posture of the ankle joint is not considered, and the position of the end lower leg is defined as the ankle joint. The position expression in the base frame is given, as shown in Formula (2).

$$\begin{cases} p_x = d_1c_1s_2 + L_2(c_5(s_1s_3c_4 + c_1c_2c_3c_4) + c_1s_2s_5) \\ p_y = d_1c_2 + L_2(c_2s_5 - s_2c_5c_3c_4) \\ p_z = d_1s_1s_2 - L_2(c_5(c_1s_3c_4 - c_1c_2c_3c_4) - s_1s_2c_5) \end{cases} \tag{2}$$

where $s_i = \sin \theta_i$, $c_i = \cos \theta_i$, $s_{ij} = \sin(\theta_i + \theta_j)$, and $c_{ij} = \cos(\theta_i + \theta_j)$ ($i, j = 1, 2, 3, 4, 5, 6$).

Assume that the position vector of the hip joint is $p_o = [x_o \ y_o \ z_o]^T$ in the global coordinate system, when the knee joint is not bent, only the hip joint is subject to rehabilita-

tion training, that is, $\vartheta_3 = -90, \vartheta_4 = 0, \vartheta_5 = 90, \vartheta_6 = 0$, let $d_1 + L_2 = b$, at this time, the position p_{op} and posture R_{op} of the end lower leg are

$$\begin{cases} p_{op} = \begin{bmatrix} p_{ox} \\ p_{oy} \\ p_{oz} \end{bmatrix} = \begin{bmatrix} bc_1s_2 \\ bc_2 \\ bs_1s_2 \end{bmatrix} + \begin{bmatrix} x_o \\ y_o \\ z_o \end{bmatrix} \\ R_{op} = \begin{bmatrix} c_1s_2 & -c_1c_2 & -s_1 \\ c_2 & s_2 & 0 \\ s_1s_2 & -s_1c_2 & c_1 \end{bmatrix} \end{cases} \quad (3)$$

By deriving both sides of the position expression in Equation (3), it can be found that the velocity v_{op} of the lower leg of the human body is

$$v_{op} = \begin{bmatrix} \dot{p}_{ox} \\ \dot{p}_{oy} \\ \dot{p}_{oz} \end{bmatrix} = \begin{bmatrix} v_{ox} \\ v_{oy} \\ v_{oz} \end{bmatrix} = \begin{bmatrix} -bs_1s_2 & bc_1s_2 \\ 0 & -bs_2 \\ bc_1s_2 & bs_1c_2 \end{bmatrix} \begin{bmatrix} \dot{\vartheta}_1 \\ \dot{\vartheta}_2 \end{bmatrix} = K\dot{\vartheta} \quad (4)$$

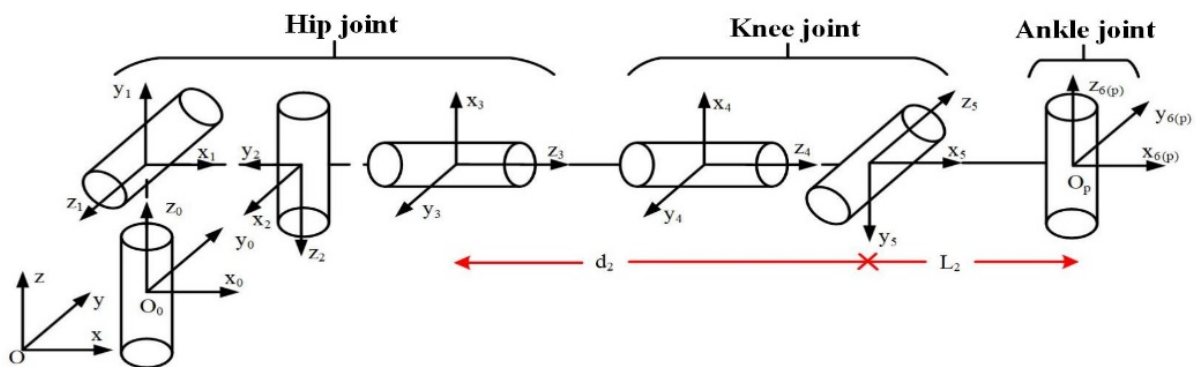


Figure 2. D–H coordinate system of human lower limbs.

Table 1. Lower limb D–H parameter.

Joint (i)	$\alpha_{i-1}/(\circ)$	L_{i-1}/cm	d_i/cm	$\vartheta_i/(\circ)$	Human Joint Limits/(\circ)
1	90	0	0	ϑ_1	0–60
2	90	0	0	ϑ_2	60–135
3	90	0	0	ϑ_3	–135 to –45
4	0	0	d_1	ϑ_4	–10 to 10
5	90	0	0	ϑ_5	90–210
6	0	L_2	0	ϑ_6	–20 to 45

By further derivation of Equation (4), the acceleration a_{op} at the end of the lower leg of the human body can be obtained as

$$a_{op} = \begin{bmatrix} \dot{v}_{ox} \\ \dot{v}_{oy} \\ \dot{v}_{oz} \end{bmatrix} = \begin{bmatrix} a_{ox} \\ a_{oy} \\ a_{oz} \end{bmatrix} = K \begin{bmatrix} \ddot{\vartheta}_1 \\ \ddot{\vartheta}_2 \end{bmatrix} + \vartheta_v^T V \vartheta_v \quad (5)$$

where

$$V = \begin{bmatrix} V_1 \\ V_2 \\ V_3 \end{bmatrix} = \begin{bmatrix} \begin{bmatrix} -bc_1s_2 & -bs_1c_2 \\ -bs_1c_2 & -bc_1s_2 \end{bmatrix} \\ \begin{bmatrix} 0 & 0 \\ 0 & -bc_2 \end{bmatrix} \\ \begin{bmatrix} -bs_1s_2 & -bc_1c_2 \\ -bc_1c_2 & -bs_1s_2 \end{bmatrix} \end{bmatrix} \quad \vartheta_v^T = \begin{bmatrix} \begin{bmatrix} \dot{\vartheta}_1 \\ \dot{\vartheta}_2 \end{bmatrix}^T \\ \begin{bmatrix} \dot{\vartheta}_1 \\ \dot{\vartheta}_2 \end{bmatrix}^T \\ \begin{bmatrix} \dot{\vartheta}_1 \\ \dot{\vartheta}_2 \end{bmatrix}^T \end{bmatrix} \quad \vartheta_v = \begin{bmatrix} \begin{bmatrix} \dot{\vartheta}_1 \\ \dot{\vartheta}_2 \end{bmatrix} \\ \begin{bmatrix} \dot{\vartheta}_1 \\ \dot{\vartheta}_2 \end{bmatrix} \\ \begin{bmatrix} \dot{\vartheta}_1 \\ \dot{\vartheta}_2 \end{bmatrix} \end{bmatrix} \quad (6)$$

3. Kinematics Analysis of Rehabilitation Robot

The robot needs to complete the required actions smoothly and accurately. First, the kinematics of the robot is analyzed, and the kinematic model of the robot is established. The rehabilitation robot with m cables is shown in Figure 3a. Figure 3b shows a free body diagram of the lower limb of three cables; W_1 , W_2 , and W_3 are the tension of the cables; and G is the gravitational force on the lower limb; when the tension of one of the cables increases, the lower limbs will move in the direction of the cable tension. The cables are made of lighter materials, ignoring their own weight and sagging [37,38]; therefore, the cable between the cable winder and the end limb can be regarded as a straight line.

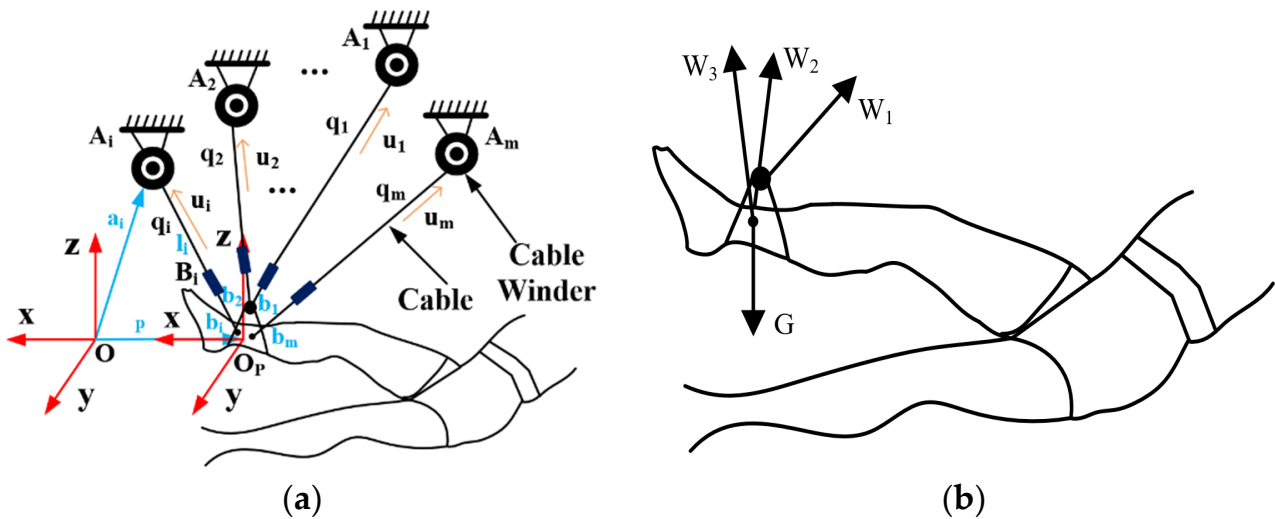


Figure 3. (a) Kinematics model. (b) Lower limb free body diagram of three cables.

In Figure 3a, $\{O - xyz\}$ is the global coordinate system, which is fixed on the first column and is always fixed during rehabilitation training, and O is its coordinate origin; $\{O_p - xyz\}$ is the local coordinate system, which is the central point at the end of the lower leg. It moves with the central point during movement, and O_p is its coordinate origin. The pose of $O_p - xyz$ at $O - xyz$ can be written as $X = [p_{op}^T \ \phi_{op}^T]^T$, $p_{op} = [p_{xop} \ p_{yop} \ p_{zop}]^T$, and $\phi_{op} = [\alpha \ \beta \ \gamma]^T$ is the position and orientation vector of the central point of the end lower leg, respectively, and α , β , and γ represent the rotation angle of the end lower leg around the x , y , and z axes of the local coordinate system. The variable A_i is the joint point between the cable and the cable winder, B_i is the joint point between the cable and the flexible belt, q_i is the length of the cable, l_i is the vector of the cable length, $u_i = l_i/q_i$ is the unit vector of the cable, and ${}^O P$ represents the rotation matrix from the local to global coordinate system. The position vector of point A_i in the global coordinate system is denoted by a_i , and the position vector of point B_i in the local coordinate system is denoted by b_i .

From the inverse posture solution, the posture of the end lower leg can be obtained as

$$\alpha = \arctan \frac{-s_1 c_2}{c_1} \quad \beta = \arctan \frac{-s_1 s_2}{\sqrt{c_1^2 s_2^2 + c_2^2}} \quad \gamma = \arctan \frac{c_2}{c_1 s_2} \quad (7)$$

From the posture of the end lower leg, we can obtain the angular velocity vector $\omega_p = [\omega_{px} \ \omega_{py} \ \omega_{pz}]^T$ of the central point relative to the local coordinate system as

$$\begin{cases} \omega_{px} = \dot{\alpha} = \frac{c_1 s_1 s_2 \dot{\theta}_2 - c_2 \dot{\theta}_1}{c_1^2 + s_1^2 c_2^2} \\ \omega_{py} = \dot{\beta} = \frac{(-c_1 s_2 \dot{\theta}_1 - s_1 c_2 \dot{\theta}_2) \sqrt{c_1^2 s_2^2 + c_2^2} + s_1 s_2 \dot{d}}{c_1^2 s_2^2 + c_2^2} \\ \omega_{pz} = \dot{\gamma} = \frac{s_1 s_2 c_2 \dot{\theta}_2 - c_1 \dot{\theta}_1}{c_1^2 s_2^2 + c_2^2} \end{cases} \quad (8)$$

angular acceleration vector $\varepsilon_p = [\varepsilon_{px} \quad \varepsilon_{py} \quad \varepsilon_{pz}]^T$ is

$$\begin{cases} \varepsilon_{px} = \dot{\omega}_{px} = \frac{N_1 - 2N_2}{(c_1^2 + c_2^2 s_1^2)^2} \\ \varepsilon_{py} = \dot{\omega}_{py} = N_3 + s_1 s_2 \ddot{d} \\ \varepsilon_{pz} = \dot{\omega}_{pz} = \frac{N_4 - 2N_5}{(c_1^2 s_2^2 + c_2^2)^2} \end{cases} \quad (9)$$

where

$$\begin{aligned} N_1 &= (c_1^2 + c_2^2 s_1^2)((2c_1^2 - s_1^2 + s_2)\dot{\theta}_1\dot{\theta}_2 + s_1 c_1 c_2 \dot{\theta}_2^2 + s_1 c_1 s_2 \ddot{\theta}_2 - c_2 \ddot{\theta}_1) \\ N_2 &= s_1(c_2 \dot{\theta}_1 - c_1 s_1 s_2 \dot{\theta}_2)(s_1 s_2 c_2 \dot{\theta}_1 + c_1 s_2^2 \dot{\theta}_1) \\ N_3 &= (s_1 s_2(\dot{\theta}_1 + \dot{\theta}_2) - 2c_1 c_2 \dot{\theta}_1 \dot{\theta}_2) \sqrt{c_1^2 s_2^2 + c_2^2} \\ N_4 &= (c_1^2 s_2^2 + c_2^2)(s_1 c_2^2 \dot{\theta}_2^2 + c_1 c_2 s_2 \dot{\theta}_1 \dot{\theta}_2 + s_1 c_2 s_2 \ddot{\theta}_2 + s_1 \dot{\theta}_1^2 - s_1 s_2^2 \dot{\theta}_2^2 - c_1 \ddot{\theta}_1) \\ N_5 &= s_2(c_1 \dot{\theta}_1 - s_1 s_2 c_2 \dot{\theta}_2)(s_1 s_2 c_1 \dot{\theta}_1 + c_2 s_1^2 \dot{\theta}_2) \\ N_6 &= (-4c_1 c_2 s_1 s_2 \dot{\theta}_1 \dot{\theta}_2 + (s_2^4 - c_2^2 s_2^2) \dot{\theta}_2^2 + s_2^2(1 - c_1 s_1) \dot{\theta}_1^2 - c_2 s_2^3 \ddot{\theta}_2) \sqrt{c_1^2 s_2^2 + c_2^2} \\ N_7 &= (-s_1^2 s_2 c_2 \dot{\theta}_2 - s_2^2 c_1 s_1 \dot{\theta}_1) \ddot{d} \\ \ddot{d} &= \frac{-s_1^2 s_2 c_2 \dot{\theta}_2 - s_2^2 c_1 s_1 \dot{\theta}_1}{\sqrt{c_1^2 s_2^2 + c_2^2}} \dots \ddot{d} = \frac{N_6 - N_7}{c_1^2 s_2^2 + c_2^2} \end{aligned} \quad (10)$$

Assuming that the angular velocity vector of the end lower leg relative to the global coordinate system is $\omega = [\omega_x \quad \omega_y \quad \omega_z]^T$ and the angular acceleration vector is $\varepsilon = [\varepsilon_x \quad \varepsilon_y \quad \varepsilon_z]^T$, the motion velocity vector is $\dot{X}_a = [v_x \quad v_y \quad v_z \quad \omega_x \quad \omega_y \quad \omega_z]^T$, which can be obtained from the principle of kinematics

$$\dot{X}_a = \begin{bmatrix} v \\ \omega \end{bmatrix} = \begin{bmatrix} I_{3 \times 3} & 0_{3 \times 3} \\ 0_{3 \times 3} & \Lambda \end{bmatrix} \dot{X} \quad (11)$$

where

$$\Lambda = \begin{bmatrix} \cos \beta \cos \gamma & -\sin \gamma & 0 \\ \cos \beta \sin \gamma & \cos \gamma & 0 \\ -\sin \beta & 0 & 1 \end{bmatrix} \dots \dot{X} = \begin{bmatrix} v \\ \omega_p \end{bmatrix} \quad (12)$$

so there are $\omega = E\omega_p$, further available

$$\varepsilon = \dot{E}\omega_p + E\varepsilon_p \quad (13)$$

Furthermore, the cable length vector can be obtained by the closed vector method,

$$l_i = a_i - p_{op} - {}^O_P R b_i, \quad (14)$$

the length of the cable is

$$q_i = \|l_i\| = \|a_i - p_{op} - {}^O_P R b_i\|, \quad (15)$$

and the quantity product of Equation (15) can be obtained as

$$q_i^2 = (l_i)^T l_i = (a_i - p_{op} - {}^O_P R b_i)^T (a_i - p_{op} - {}^O_P R b_i) \quad (16)$$

In the process of rehabilitation training, as cable winder A_i will move on the rail bracket, vector a_i will change, the derivation is not zero, point B_i is fixed relative to the local coordinate system, vector b_i is a fixed value, and its derivative is zero. The derivation of time on both sides of Equation (16) is simplified

$$q_i \dot{q}_i = (l_i)^T (\dot{a}_i - \dot{p}_{op} - {}^O_P \dot{R} b_i) \quad (17)$$

due to ${}^O_P\dot{R}b_i = \omega \times {}^O_P Rb_i$, Equation (17) can be written as

$$q_i \dot{q}_i = (l_i)^T (\dot{a}_i - \dot{p}_{op} - \omega \times {}^O_P Rb_i) \tag{18}$$

Equation (18) divides both sides by q_i , and the cable length speed is

$$\begin{aligned} \dot{q}_i &= u_i^T (\dot{a}_i - \dot{p}_{op} - \omega \times {}^O_P Rb_i) \\ &= -u_i^T \dot{p}_{op} - ({}^O_P Rb_i \times u_i)^T \omega + u_i^T \dot{a}_i \end{aligned} \tag{19}$$

by substituting (4) into (19),

$$\dot{q}_i = -u_i^T K \dot{\theta} - ({}^O_P Rb_i \times u_i)^T \omega + u_i^T \dot{a}_i \tag{20}$$

Therefore, the relationship between the joint angle, moving velocity of the cable winder and velocity of the cable is

$$\dot{q} = -\Xi_k \dot{\Psi} + \Xi_a \dot{A} \tag{21}$$

where

$$\Xi_k = \begin{bmatrix} (u_1^T K)^T & (u_2^T K)^T & (u_3^T K)^T & \dots & (u_m^T K)^T \\ {}^O_P Rb_1 \times u_1 & {}^O_P Rb_2 \times u_2 & {}^O_P Rb_3 \times u_3 & \dots & {}^O_P Rb_m \times u_m \end{bmatrix}^T \in R^{m \times 5},$$

which is the first-order influence coefficient matrix of cable motion on hip motion.

$$\Xi_a = [[u_1^T] \quad [u_2^T] \quad [u_3^T] \quad \dots \quad [u_m^T]]^T \tag{22}$$

$$\dot{A} = \begin{bmatrix} [\dot{a}_1] \\ [\dot{a}_2] \\ [\dot{a}_3] \\ \dots \\ [\dot{a}_m] \end{bmatrix} \dots \dot{\Psi} = \begin{bmatrix} \dot{\theta} \\ \omega \end{bmatrix} \tag{23}$$

By deriving the time at both ends of Equation (21), the kinematic acceleration of the cable-driven rehabilitation robot can be obtained as

$$\ddot{q} = -\Xi_k \ddot{\Psi} - \dot{\Xi}_k \dot{\Psi} + \Xi_a \ddot{A} + \dot{\Xi}_a \dot{A} \tag{24}$$

where

$$\dot{\Xi}_k = \begin{bmatrix} ((\omega \times u_1)^T K + u_1^T (\vartheta_v^T V))^T & \dots & ((\omega \times u_m)^T K + u_m^T (\vartheta_v^T V))^T \\ \omega \times ({}^O_P Rb_1) \times u_1 + ({}^O_P Rb_1) \times (\omega \times u_1) & \dots & \omega \times ({}^O_P Rb_m) \times u_m + ({}^O_P Rb_m) \times (\omega \times u_m) \end{bmatrix}^T \tag{25}$$

$$\dot{\Xi}_a = [[\omega \times u_1]^T \quad [\omega \times u_2]^T \quad [\omega \times u_3]^T \quad \dots \quad [\omega \times u_m]^T]^T \dots \dot{\Psi} = \begin{bmatrix} \ddot{\theta} \\ \varepsilon \end{bmatrix} \tag{26}$$

In summary, the kinematics of the rehabilitation robot are obtained through Equations (15), (21) and (24). The change in cable length is related to the position and orientation of the end lower leg, that is, the angle of the human hip joint. In the range of motion of the hip joint, reasonably plan the joint angle and inversely solve the orientation of the end lower leg through the analysis of kinematics theory, then the corresponding relationship between the angle change of human hip joint and the change of each cable can be obtained. Therefore, according to the angle relationship of the hip joint movement, the length change and motion law of the cable in the system can be obtained.

4. Trajectory Planning

4.1. Adaptive S-Shaped Speed Curve

To improve the rehabilitation effect of patients, it is necessary to adopt different rehabilitation training modes, reasonably plan rehabilitation actions, and carry out targeted rehabilitation training. Because leg length varies from person to person, it is necessary to carry out trajectory planning in joint space, and then map to the cable length space of the system through kinematics theory. The adaptive S-shaped speed curve can reduce the impact on the control process during the movement of the robot, the whole process is relatively flexible, and the whole curve has seven stages [39]. The adaptive S-shaped speed curve adaptively adjusts the value of each time according to the parameters. Suppose we know that the maximum speed ζ_v , the maximum acceleration ζ_a and the total running time T during the movement, the initial displacement is l_0 , the total running length is h , and the intermediate variable $s(t)$ is introduced, which is a function of time. The domain is $[0, T]$, the value range is $[0, 1]$, and the expression of $s(t)$ is

$$s(t) = \begin{cases} \frac{1}{6}\zeta_J t^3 & 0 \leq t < \partial_1 \\ \frac{1}{2}\zeta_a(t - \partial_1)^2 + \frac{\zeta_a^2}{2\zeta_J}(t - \partial_1) + \frac{\zeta_a^3}{6\zeta_J^2} & \partial_1 \leq t < \partial_2 \\ -\frac{1}{6}\zeta_J(t - \partial_2)^3 + \frac{1}{2}\zeta_a(t - \partial_2)^2 + (\zeta_a t_2 + \frac{\zeta_a^2}{2\zeta_J})(t - \partial_2) + \frac{1}{2}\zeta_a t_2^2 + \frac{\zeta_a^2}{2\zeta_J} t_2 + \frac{\zeta_a^3}{6\zeta_J^2} & \partial_2 \leq t < \partial_3 \\ (-\frac{1}{2}\zeta_J t_3^2 + \zeta_a t_3 + \zeta_a t_2 + \frac{\zeta_a^2}{2\zeta_J})(t - \partial_3) - \frac{1}{6}\zeta_J t_3^3 + \frac{1}{2}\zeta_a t_3^2 + (\zeta_a t_2 + \frac{\zeta_a^2}{2\zeta_J}) t_3 + \frac{1}{2}\zeta_a t_2^2 + \frac{\zeta_a^2}{2\zeta_J} t_2 + \frac{\zeta_a^3}{6\zeta_J^2} & \partial_3 \leq t < \partial_4 \\ 1 + \frac{1}{6}\zeta_J(T - t - \partial_2)^3 - \frac{1}{2}\zeta_a(T - t - \partial_2)^2 - (\zeta_a t_2 + \frac{\zeta_a^2}{2\zeta_J})(T - t - \partial_2) - \frac{1}{2}\zeta_a t_2^2 - \frac{\zeta_a^2}{2\zeta_J} t_2 - \frac{\zeta_a^3}{6\zeta_J^2} & \partial_4 \leq t < \partial_5 \\ 1 - \frac{1}{2}\zeta_a(T - t - \partial_1)^2 - \frac{\zeta_a^2}{2\zeta_J}(T - t - \partial_1) - \frac{\zeta_a^3}{6\zeta_J^2} & \partial_5 \leq t < \partial_6 \\ 1 - \frac{1}{6}\zeta_J(T - t)^3 & \partial_6 \leq t < \partial_7 \end{cases} \tag{27}$$

where $T = \tau_7 = t_1 + t_2 + t_3 + t_4 + t_5 + t_6 + t_7$, $\zeta_J = \frac{\zeta_a^2 \zeta_v}{T \zeta_v \zeta_a - \zeta_v^2 - \zeta_a}$ represents jerk, $\partial_k (k = 1, 2, \dots, 7)$ represents the moment when the k th segment of the movement process ends, and $t_k (k = 1, 2, \dots, 7)$ represents the time required for the k th segment displacement, where $t_1 = \frac{\zeta_a}{\zeta_J}$, $t_2 = \frac{\zeta_v}{\zeta_a} - \frac{\zeta_a}{\zeta_J}$, $t_3 = \frac{\zeta_a}{\zeta_J}$, $t_4 = T - \frac{2\zeta_a}{\zeta_J} - \frac{2\zeta_v}{\zeta_a}$, $t_5 = t_3$, $t_6 = t_2$, $t_7 = t_1$. Therefore, the joint angular displacement, velocity, and acceleration of the S-shaped velocity curve are

$$\begin{cases} l(t) = l_0 + sh \\ \zeta_v(t) = \dot{s}h \\ \zeta_a(t) = \ddot{s}h \end{cases} \tag{28}$$

4.2. Polynomial Programming Based on S-Shaped Curve

For rehabilitation training with patient participation, the rehabilitation action is mainly repetitive action, which should ensure that the rehabilitation patients feel comfortable, and the motion curve should be smooth to avoid a large impact. Therefore, the cable length should change continuously, and the cable tension should be smooth. The acceleration of cable length will affect the cable tension, so it is very meaningful to analyze the acceleration change of cable length. The S-shaped curve is selected to plan the trajectory, and the displacement, velocity, and acceleration curves are stable, but there is still a problem of poor compliance in the acceleration and deceleration stages. However, with polynomial planning, most of the speed curves obtained are acceleration and deceleration sections. For rehabilitation patients, there is a certain uniform stage in the initial stage of rehabilitation, which is more conducive to the recovery of limb movement. Therefore, a quintic polynomial programming method based on an S-shaped curve is proposed in this paper. First, the S-shaped speed curve is selected to plan the middle point, and then the obtained middle point speed is used to optimize the acceleration and deceleration stage of the path with quintic polynomial interpolation. The planning flow chart is shown in Figure 4. We directly

plan the trajectory of human joints. According to the kinematic analysis of the rehabilitation robot, the joint angle will affect the change of the cable, the change of the cable will directly affect the trajectory in task space by the closed vector method, therefore, the smooth change of the cable will make the smooth change of the trajectory in task space.

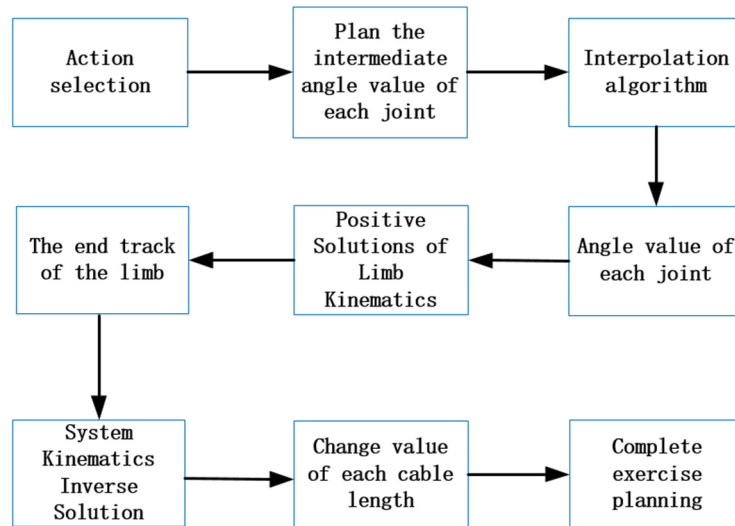


Figure 4. Planning process.

Taking the joint angle as a function of time, the expressions of angular displacement, angular velocity, and angular acceleration are

$$\begin{aligned}
 \vartheta(t) &= \kappa_0 + \kappa_1 t + \kappa_2 t^2 + \kappa_3 t^3 + \kappa_4 t^4 + \kappa_5 t^5 \\
 \dot{\vartheta}(t) &= \kappa_1 + 2\kappa_2 t + 3\kappa_3 t^2 + 4\kappa_4 t^3 + 5\kappa_5 t^4 \\
 \ddot{\vartheta}(t) &= 2\kappa_2 + 6\kappa_3 t + 12\kappa_4 t^2 + 20\kappa_5 t^3
 \end{aligned} \tag{29}$$

the conditions to be met in the initial stage are

$$\begin{aligned}
 \vartheta(0) &= \vartheta_0, \dot{\vartheta}(0) = 0, \ddot{\vartheta}(0) = 0 \\
 \vartheta(\partial_3) &= \vartheta_{\partial_3}, \dot{\vartheta}(\partial_3) = v, \ddot{\vartheta}(\partial_3) = 0
 \end{aligned} \tag{30}$$

the conditions to be met in the termination stage are

$$\begin{aligned}
 \vartheta(\partial_4) &= \vartheta_{\partial_4}, \dot{\vartheta}(\partial_4) = v, \ddot{\vartheta}(\partial_4) = 0 \\
 \vartheta(\partial_7) &= \vartheta_{\partial_7}, \dot{\vartheta}(\partial_7) = 0, \ddot{\vartheta}(\partial_7) = 0
 \end{aligned} \tag{31}$$

the joint displacement can be obtained by simultaneous (29)–(31)

$$\vartheta(t) = \begin{cases} \vartheta_0 + \frac{10(\vartheta_{\partial_3} - \vartheta_0) - 4v\partial_3}{\partial_3^3} t^3 + \frac{15(\vartheta_0 - \vartheta_{\partial_3}) - 7v\partial_3}{\partial_3^4} t^4 + \frac{6(\vartheta_{\partial_3} - \vartheta_0) - 3v\partial_3}{\partial_3^5} t^5 & 0 \leq t < \partial_3 \\ \vartheta_{\partial_3} + sh & \partial_3 \leq t < \partial_4 \\ \vartheta_{\partial_4} + vt + \frac{10(\vartheta_{\partial_7} - \vartheta_{\partial_4}) - 6v\partial_7}{\partial_7^3} t^3 + \frac{15(\vartheta_0 - \vartheta_{\partial_7}) + 8v\partial_7}{\partial_7^4} t^4 + \frac{6(\vartheta_{\partial_7} - \vartheta_{\partial_4}) - 3v\partial_7}{\partial_7^5} t^5 & \partial_4 \leq t < \partial_7 \end{cases} \tag{32}$$

the joint angular velocity is

$$\dot{\vartheta}(t) = \begin{cases} \frac{30(\vartheta_{\partial_3} - \vartheta_0) - 12v\partial_3}{\partial_3^3} t^2 + \frac{60(\vartheta_0 - \vartheta_{\partial_3}) - 28v\partial_3}{\partial_3^4} t^3 + \frac{30(\vartheta_{\partial_3} - \vartheta_0) - 15v\partial_3}{\partial_3^5} t^4 & 0 \leq t < \partial_3 \\ sh & \partial_3 \leq t < \partial_4 \\ v + \frac{30(\vartheta_{\partial_7} - \vartheta_{\partial_4}) - 18v\partial_7}{\partial_7^3} t^2 + \frac{60(\vartheta_0 - \vartheta_{\partial_7}) + 32v\partial_7}{\partial_7^4} t^3 + \frac{30(\vartheta_{\partial_7} - \vartheta_{\partial_4}) - 15v\partial_7}{\partial_7^5} t^4 & \partial_4 \leq t < \partial_7 \end{cases} \tag{33}$$

the joint angular acceleration is

$$\ddot{\theta}(t) = \begin{cases} \frac{60(\theta_{\partial_3} - \theta_0) - 24v\partial_3}{\partial_3^3} t + \frac{180(\theta_0 - \theta_{\partial_3}) - 84v\partial_3}{\partial_3^4} t^2 + \frac{120(\theta_{\partial_3} - \theta_0) - 60v\partial_3}{\partial_3^5} t^3 & 0 \leq t < \partial_3 \\ \ddot{\theta}h & \partial_3 \leq t < \partial_4 \\ \frac{60(\theta_{\partial_7} - \theta_{\partial_4}) - 36v\partial_7}{\partial_7^3} t + \frac{180(\theta_0 - \theta_{\partial_7}) + 96v\partial_7}{\partial_7^4} t^2 + \frac{120(\theta_{\partial_7} - \theta_{\partial_4}) - 60v\partial_7}{\partial_7^5} t^3 & \partial_4 \leq t < \partial_7 \end{cases} \quad (34)$$

where $\theta_{\partial_k}, \dot{\theta}_{\partial_k}, \ddot{\theta}_{\partial_k} (k = 1, 2, \dots, 7)$ are the angle, velocity, and acceleration at time ∂_k , respectively.

5. Simulation Results

To verify the effectiveness and feasibility of the proposed planning algorithm, the simulation test is carried out with a rehabilitation robot platform driven by three cable certificates. Figure 5 shows the cable-driven rehabilitation robot platform. The size of the robot is 200 cm * 160 cm * 200 cm. The movement of the cable winders will change the working space and performance of the robot. The control strategy adopted in this study is as follows: set one cable winder as a fixed point, its coordinates in the global coordinate system are $a_1 = [40 \text{ cm}, 80 \text{ cm}, 200 \text{ cm}]^T$, and the other two cable winders move with the end limbs on the rail brackets, and the coordinates are $a_2 = [x_2, 0, 200 \text{ cm}]^T$, $a_3 = [x_3, 160 \text{ cm}, 200 \text{ cm}]^T$, that is, $x_2 = x_3$. The position of the connection point of the cable and the flexible belt in the local coordinate system is $b_1 = [0, 0, 5 \text{ cm}]^T$, $b_2 = [0, -4 \text{ cm}, 0]^T$, $b_3 = [0, 4 \text{ cm}, 0]^T$. According to the body size of a normal adult human, the length of thigh d_1 is estimated as 50 cm and the length of lower leg L_2 is 40 cm. To achieve a better rehabilitation effect, three point-to-point paths are planned, and the planning time for each path is 6 s. The angular displacement, maximum angular velocity, and maximum angular acceleration of joint 1 and joint 2 are shown in Tables 2 and 3. The terminal trajectory diagram is shown in Figure 5, and it can be observed that the three paths are all arc-shaped. The desired motion starts from point D(170, 80, 80) and passes through points E(134.4, 49.2, 144.8), F(134.4, 110.8, 144.8), before finally returning to point D.

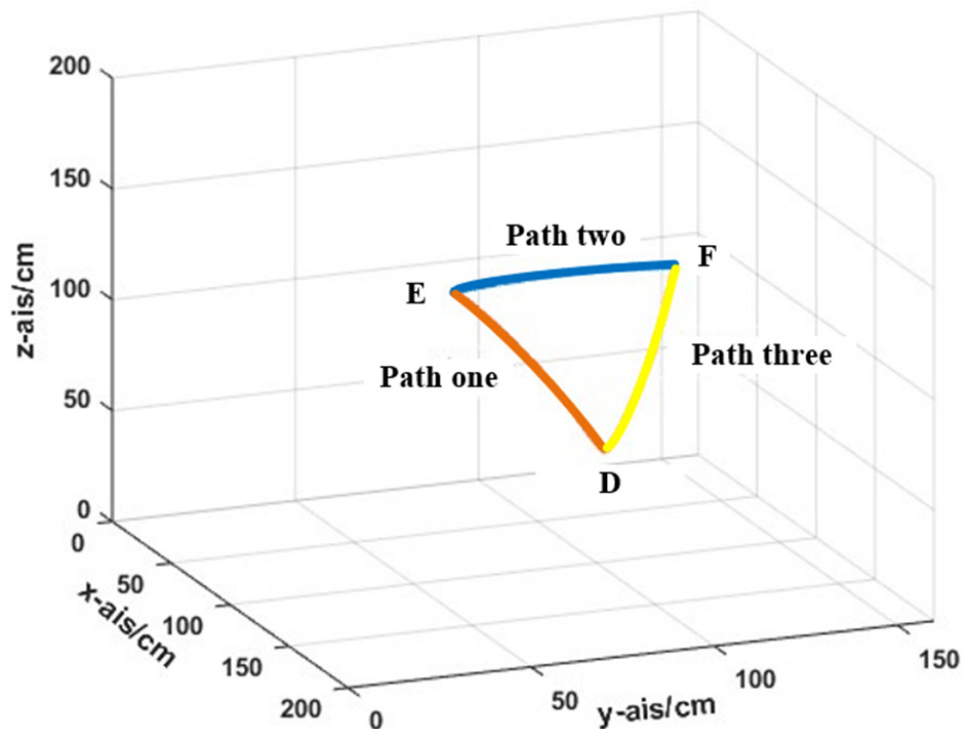


Figure 5. Terminal trajectory.

Table 2. Constraints of joint 1.

Joint 1	Angular Displacement (°)	Maximum Angular Velocity (°/s)	Maximum Angular Acceleration (°/s ²)
Path one	0–50	13	25
Path two	50–50	0	0
Path three	50–0	13	25

Table 3. Constraints of joint 2.

Joint 2	Angular Displacement (°)	Maximum Angular Velocity (°/s)	Maximum Angular Acceleration (°/s ²)
Path one	90–110	5	10
Path two	110–70	10	20
Path three	70–90	5	10

The fifth-order polynomial planning method based on the S-shaped curve is now used for hip joint spatial trajectory planning. Figure 6 shows the velocity and acceleration curves of joint 1 and joint 2 under three paths: Figure 6a,b is path one, Figure 6c,d is path two, and Figure 6e,f is path three. The joint angular velocity and acceleration on each path are within the constrained maximum joint angular velocity and acceleration range, and the start and end parts slowly transition to the final value. The middle section is a constant speed section, the whole process is relatively smooth, and there is no jitter phenomenon, which is beneficial to improve the comfort of the recovered person. Figure 7 shows the curve of the cable acceleration change under the S-shaped speed curve. The acceleration peak is large, and the smoothness of the curve is poor. Figure 8 shows the length, speed and acceleration curves of 3 cables with time under the fifth-order polynomial programming method based on the S-shaped curve. In the figure, the cable length, speed, and acceleration change curves are smooth and continuous. Due to the symmetrical path changes, cable 1 changes to a symmetrical distribution, and the remaining cable lengths have periodicity and grouping similarity; therefore, the change laws of cable two and cable three are similar. At the end of each path, the speed and acceleration are zero, and there is no sudden change. Compared with the S-shaped speed curve planning method, the fifth-order polynomial planning method based on the S-shaped curve shows stable acceleration and a smaller peak value and has a better planning effect.

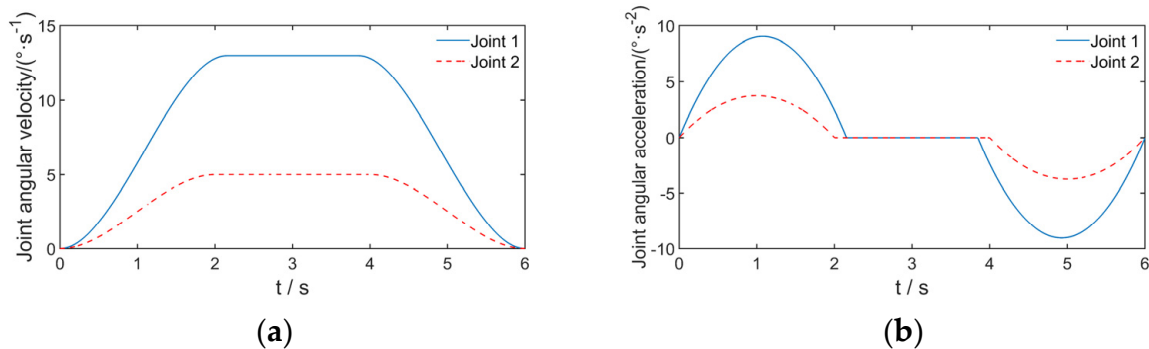


Figure 6. Cont.

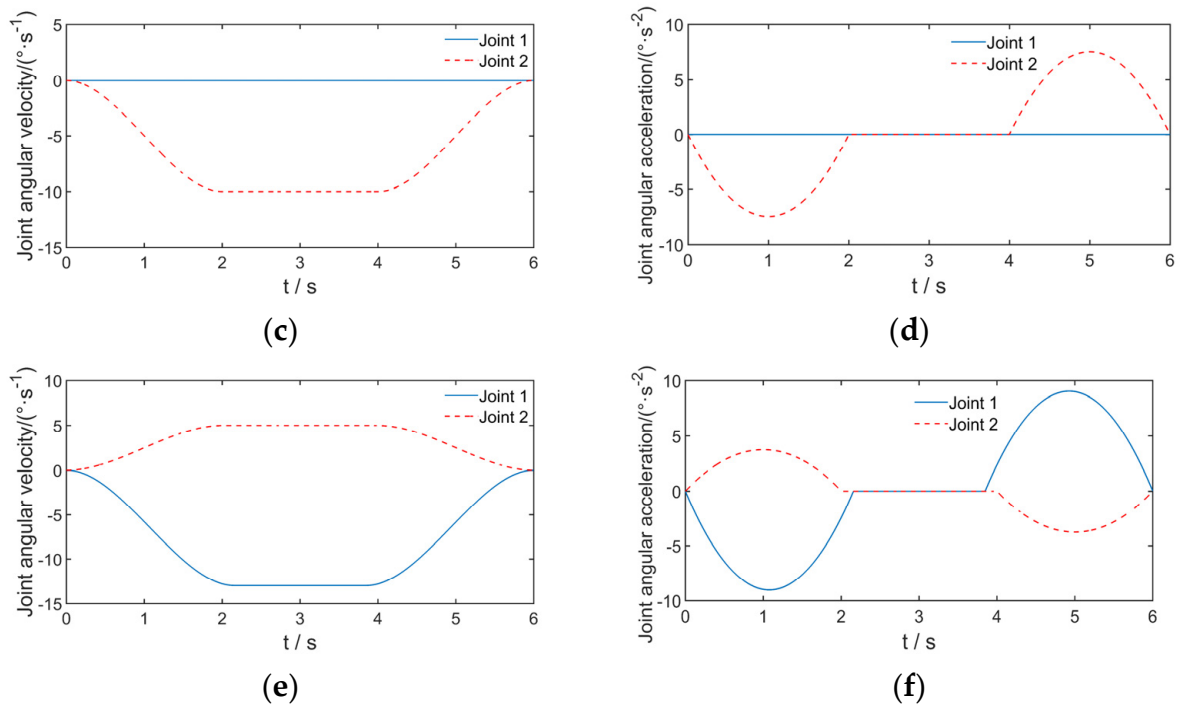


Figure 6. Joint velocity and acceleration under three paths: (a) Joint velocity of path one; (b) Joint acceleration of path one; (c) Joint velocity of path two; (d) Joint acceleration of path two; (e) Joint velocity of path three; (f) Joint acceleration of path three.

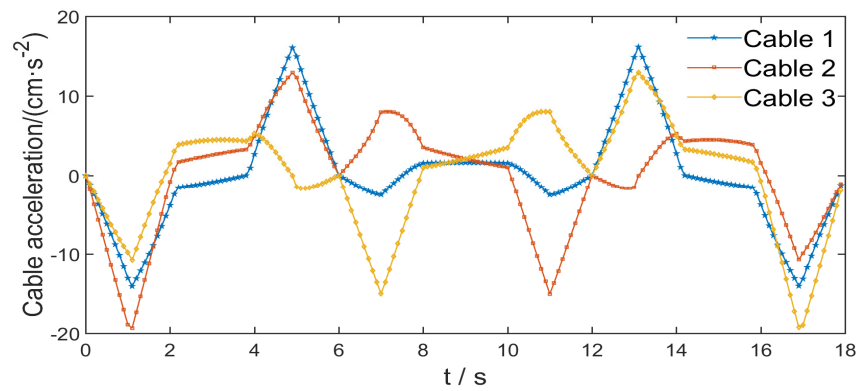


Figure 7. S-shaped acceleration of cables.

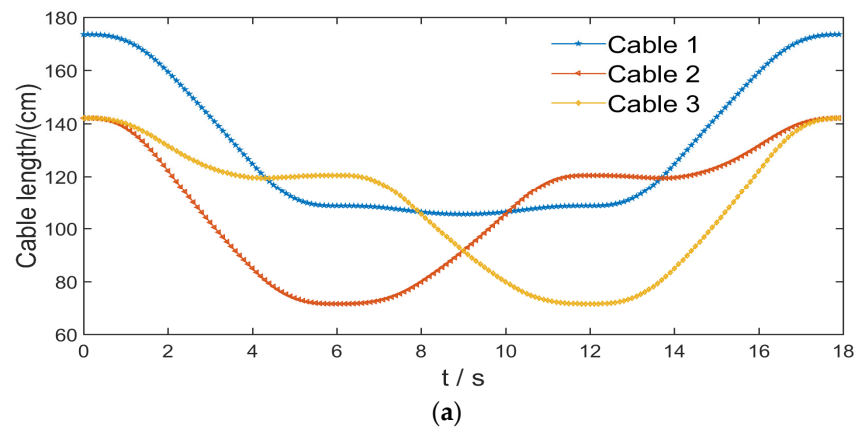


Figure 8. Cont.

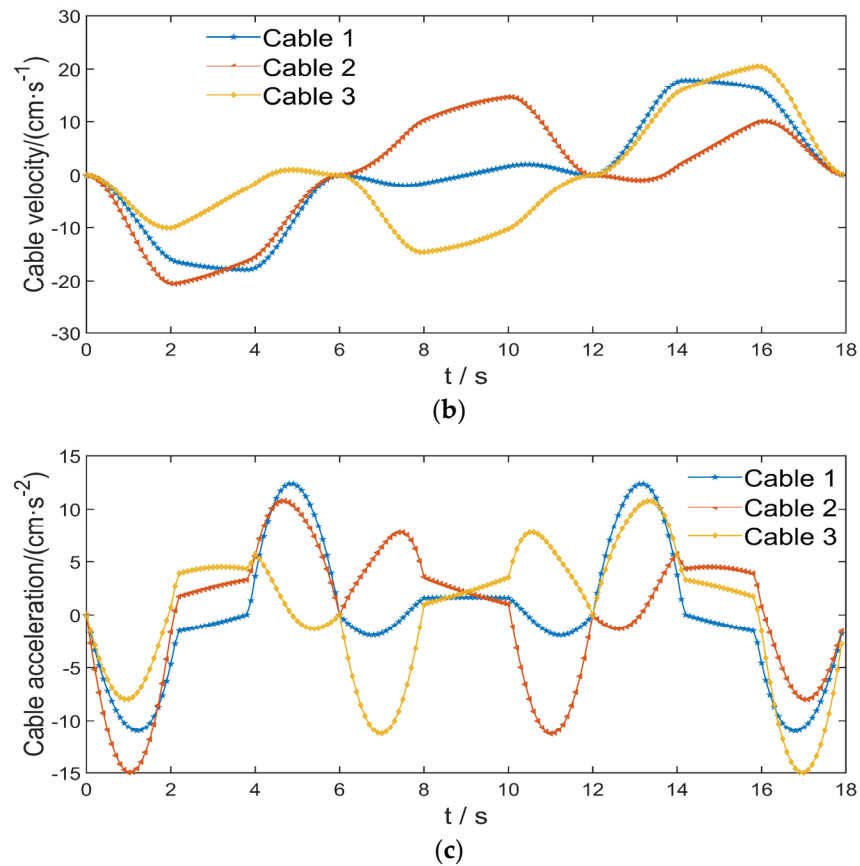


Figure 8. The cable length change based on the fifth-order polynomial of the S-shaped curve: (a) Length variation of cables; (b) Velocity variation of cables; (c) Acceleration variation of cables.

The significant optimality criteria for trajectory planning are minimum jerk and minimum energy. As the control of jerk coincides with the torque rate control, the jerk can affect the smoothness of the trajectory [40]. Reducing the jerk will lead to a smoother trajectory [41]. Limiting the jerk of the trajectory contributes to extend the life of the robot and improves tracking accuracy. The rehabilitation training process requires that the trajectory is smoother and stable and that the energy consumed by the motors is as small as possible. Smooth trajectory is easier to track and reduces the stresses to the actuators. The smoother trajectory can also improve the rehabilitation effect. Reducing energy consumption can achieve the purpose of energy saving. Similar to the work in [42], the index to measure the smoothness of the trajectory is introduced, as shown in Equation (35). The objective function is the time integral of the squared cable jerk throughout the motion. The smaller the index values are, the smoother the trajectory. The energy consumption of the motors is mainly used to drive the change of the cables. Equation (36) is an index that measures the amount of energy consumed by motors. The objective function is the time integral of the squared cable acceleration throughout the motion. The smaller the index values are, the smaller the energy consumption.

$$S_1 = \sum_{i=1}^N \sqrt{\frac{1}{H} \int_0^H L_{ji}^2 dt} \tag{35}$$

$$S_2 = \sum_{i=1}^N \sqrt{\frac{1}{H} \int_0^H L_{ai}^2 dt} \tag{36}$$

where S_1 —the index to measure the trajectory, S_2 —the index to measure the energy consumption of the motors, H —the total time for the robot to complete the task trajectory, L_{ji} —the jerk of cables, L_{ai} —the acceleration of cables, N —the number of cables, and $N = 3$.

Table 4 shows the trajectory smoothness and energy consumption under the three planning methods. The index value under fifth-order polynomial planning is the largest, $S_1 = 7.4505$, $S_2 = 29.8935$. The reason is that the planned curve does not have a uniform speed section, and the entire planning process has been in a state of acceleration and deceleration, so the energy consumption is relatively large. Compared with the S-shaped planning, the two index values under the fifth-order polynomial planning based on the S-shaped are the smallest, $S_1 = 5.8320$, $S_2 = 27.8875$. Indicating that the trajectory planned by this method is smoother and the motor consumes less energy, which is suitable for patients to perform rehabilitation training.

Table 4. Performance indicators under the three trajectory planning methods.

Index	Fifth-Degree Polynomial Programming Based on S-Curve	S-Shaped Curve	Quintic Polynomial Programming
S_1	5.8320	6.3689	7.4505
S_2	27.8875	28.0933	29.8935

6. Experiments of Rehabilitation Robot

This study carries out the experimental verification of a cable-driven rehabilitation robot platform built in the laboratory, as shown in Figure 9. The entire control process is shown in Figure 10. The PC is selected as the upper computer controller of the robot, its main configuration is Intel(R)Core(TM)i5-3210, CPU@2.50 GHz, the programming environment is MATLAB2016 (64-bit), and the controller is STM32F103ZET6 embedded processor system. The DC motor is a low-voltage type DC reducer motor DC_24V, the model number is JM-039, and its maximum load is 200 kg. The servo motor is bus type stepper motor DC_80V with high control accuracy, the model number is 86J12156EC-1000-60-SC, and its maximum torque is 12N/M. The motors selected can meet the load requirements for rehabilitation.

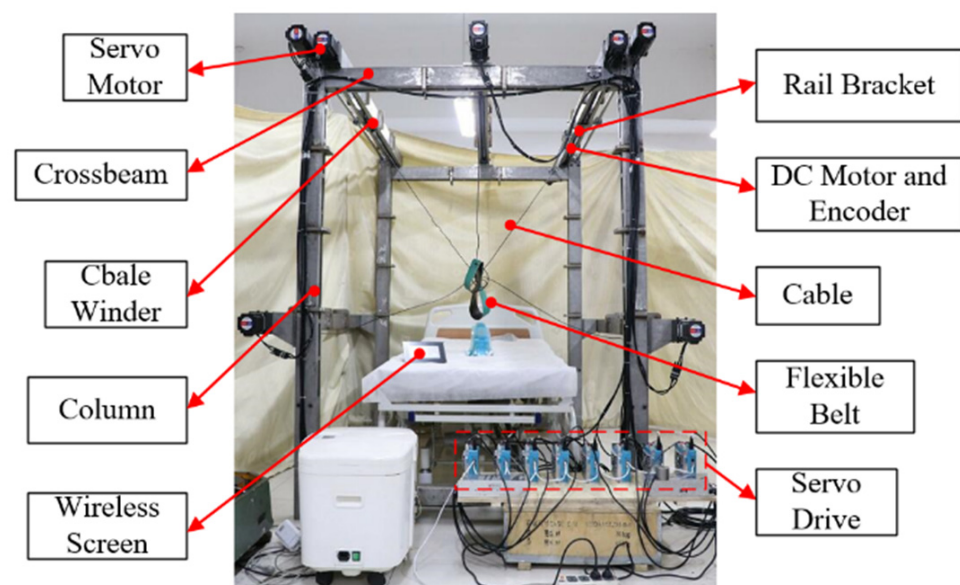


Figure 9. Experimental platform.

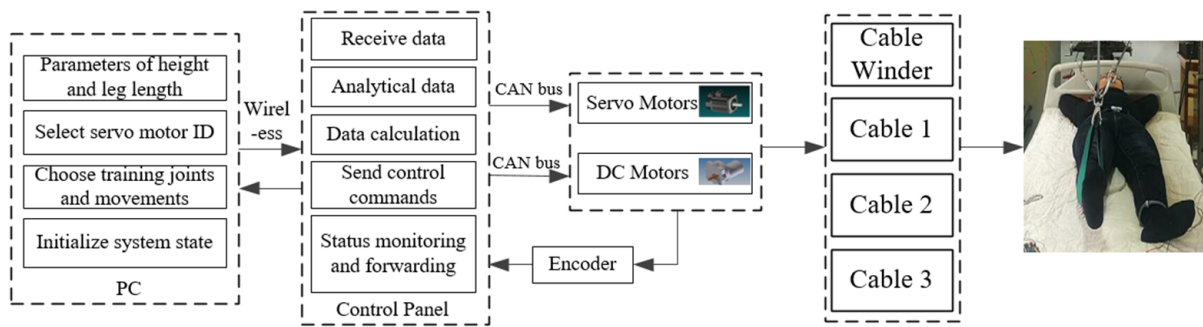


Figure 10. Control process.

First, we determine the patient’s leg length parameters and servo ID, initialize the corresponding parameters, and then the host computer and the controller send and receive data through the wireless serial port. The controller receives the data and analyzes and sends the control command to the bus by CAN communication, and the servo motors and the DC motors receive the command and perform actions.

The experimenter’s hip joint was fixed to the bed, and 3 cables were used for a cycle of rehabilitation, as shown in Figure 11. The length change of cables is measured with an absolute encoder with a resolution of 2^{10} p/r, as shown in Figures 12–14. It can be seen that there is some fluctuation in the cable length change, which may be due to the encoder jitter caused by the cable winder rotating with the cable exit point. Moreover, there will be sliding between the cables and pulleys, which may also make the cable length to fluctuate. Especially, the length of cable 1 fluctuates more seriously in path two; this occurs because cable winder A1 keeps rotating on this path. In the future work, we can improve the mechanical structure to make the rotation of the cable exit point smoother and increase the friction between the cables and the pulleys.

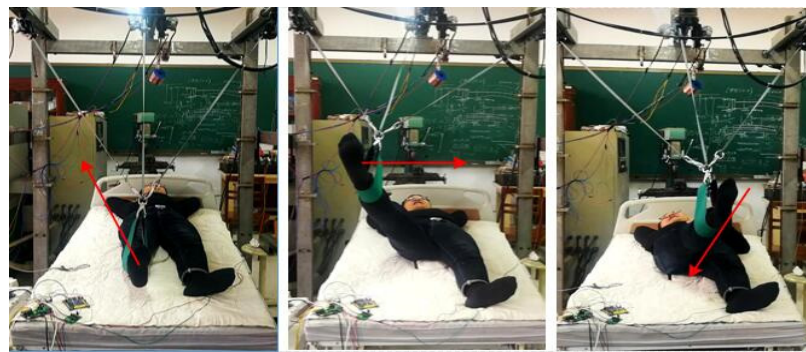


Figure 11. Experiment procedure.

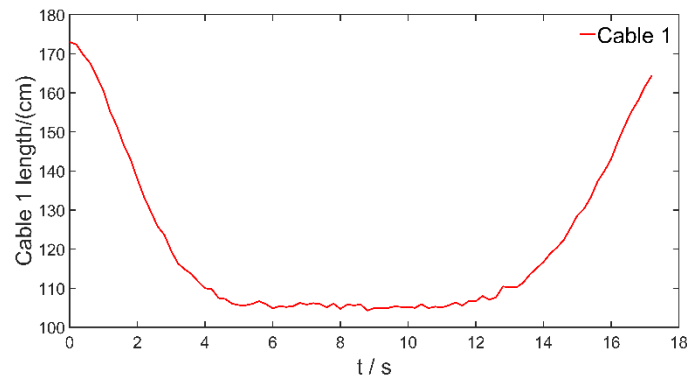


Figure 12. Length variation of cable 1.

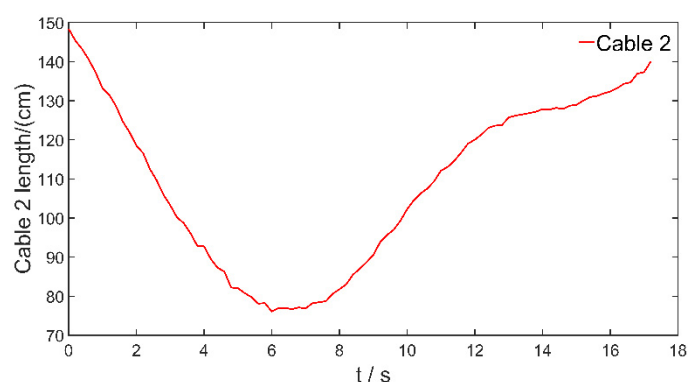


Figure 13. Length variation of cable 2.

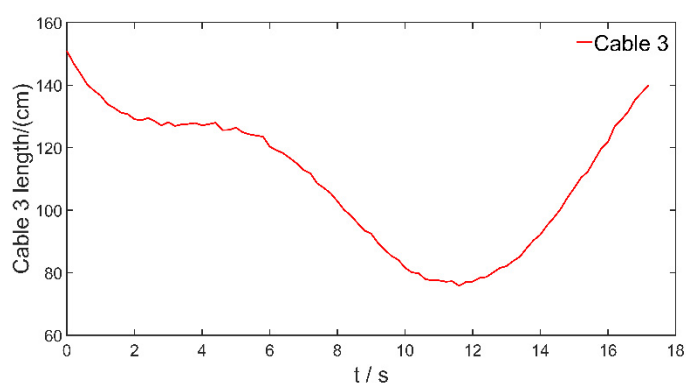


Figure 14. Length variation of cable 3.

7. Conclusions

A new type of cable-driven rehabilitation robot was designed. To achieve a better rehabilitation effect, kinematics analysis was carried out, and a new trajectory planning method was used to design the robots' motion. The feasibility of the method was verified by a simulation. The D–H method is used to derive the kinematic equations of the lower limbs when the human body is in the prone posture. When the knee joint is not bent, the displacement, speed, and acceleration of the end lower leg are analyzed. When the cable winders move along the rail bracket, a closed vector method was used to establish the kinematic model of the robot, and the relationship between the human joint angle and the cable length change was deduced. A quintic polynomial trajectory planning method based on an S-shaped curve is proposed, and the performance of the three planning methods is analyzed through two indicators. The results show that the trajectory under the new planning method is smoother, the motor consumes less energy, and it is suitable for patients' rehabilitation training. The next step is to study robot dynamics and control strategies.

Author Contributions: Conceptualization, J.Z., D.C. and Y.W.; methodology, J.Z.; software, J.Z.; validation, D.C. and Y.W.; resources, D.C.; data curation, J.Z.; writing—original draft preparation, J.Z.; writing—review and editing, J.Z., D.C. and Y.W.; visualization, J.Z.; supervision, Y.W.; project administration, D.C.; funding acquisition, D.C. and Y.W. All authors have read and agreed to the published version of the manuscript.

Funding: This research was supported in part by the National Key Research and Development Program of China under Grant 2018YFC2001704, in part by the National Natural Science Foundation of China under Grant 61703232 and Grant 62073187, in part by the Major Scientific and Technological Innovation Project in Shandong Province under Grant 2019JZZY011111, in part by the Science and Technology Innovation Special Plan Project of Rizhao under Grant 2019CXZX2212, and in part by the Jining City Key Research and Development Program Project under Grant 2020JKNS004.

Institutional Review Board Statement: All subjects gave their informed consent for inclusion before they participated in the study. The study was conducted in accordance with the Declaration of

Helsinki, and the protocol was approved by the biomedical Ethics Committee of Qufu Normal University (2021-069).

Informed Consent Statement: Informed consent was obtained from all subjects involved in the study.

Conflicts of Interest: The authors declare no conflict of interest.

References

- Chen, B.; Ma, H.; Yin, L.; Gao, F.; Chan, K.-M.; Law, S.-W.; Qin, L.; Liao, W.-H. Recent developments and challenges of lower extremity exoskeletons. *J. Orthop. Transl.* **2016**, *5*, 26–37. [\[CrossRef\]](#)
- Wang, Y.-L.; Wang, K.-Y.; Zhao, W.-Y.; Wang, W.-L.; Han, Z.; Zhang, Z.-X. Effects of single crouch walking gaits on fatigue damages of lower extremity main muscles. *J. Mech. Med. Biol.* **2019**, *19*, 1940046. [\[CrossRef\]](#)
- Zhao, Y.N.; Hao, Z.W.; Li, J.M. The effect of lokomat lower limb gait training rehabilitation robot on balance function and walking ability in hemiplegic patients after ischemic stroke. *Chin. J. Rehabil. Med.* **2012**, *27*, 1015–1020.
- Gazi, A.; Ahmet, E.C.; Erkan, K. Exoskeleton design and adaptive compliance control for hand rehabilitation. *Trans. Inst. Meas. Control.* **2019**, *42*, 493–502.
- Reinkensmeyer, D.J.; Boninger, M.L. Technologies and combination therapies for enhancing movement training for people with a disability. *J. Neuroeng. Rehabil.* **2012**, *9*, 17. [\[CrossRef\]](#) [\[PubMed\]](#)
- Wang, K.; Yin, P.; Yang, H.; Wang, L. Motion planning of rigid chain for rigid-flexible coupled robot. *Int. J. Adv. Robot. Syst.* **2018**, *15*, 1729881418772815. [\[CrossRef\]](#)
- Nef, T.; Guidali, M.; Klamroth-Marganska, V.; Riener, R. ARMin-exoskeleton robot for stroke rehabilitation. *IFMBE Proc.* **2009**, *25*, 127–130.
- Jian, H.; Tu, X.; He, J. Design and evaluation of the RUPERT wearable upper extremity exoskeleton robot for clinical and in-home therapies. *IEEE Trans. Syst. Man Cybern. Syst.* **2016**, *46*, 926–935.
- Perry, J.C.; Rosen, J. Upper-limb powered exoskeleton design. *IEEE/ASME Trans. Mechatron.* **2007**, *12*, 408–417. [\[CrossRef\]](#)
- Chen, S.H.; Lien, W.-M.; Wang, W.-W.; Lee, G.-D.; Hsu, L.-C.; Lee, K.-W.; Lin, S.-Y.; Lin, C.-H.; Fu, L.-C.; Lai, J.-S.; et al. Assistive control system for upper limb rehabilitation robot. *IEEE Trans. Neural Syst. Rehabil. Eng.* **2016**, *24*, 1199–1209. [\[CrossRef\]](#)
- Ugurlu, B.; Nishimura, M.; Hyodo, K.; Kawanishi, M.; Narikiyo, T. Proof of concept for robot-aided upper limb rehabilitation using disturbance observers. *IEEE Trans. Hum.-Mach. Syst.* **2015**, *45*, 110–118. [\[CrossRef\]](#)
- Rathore, A.; Wilcox, M.; Ramirez, D.Z.M.; Loureiro, R.; Carlson, T. Quantifying the human-robot interaction forces between a lower limb exoskeleton and healthy users. In Proceedings of the 2016 38th Annual International Conference of the IEEE Engineering in Medicine and Biology Society (EMBC), Orlando, FL, USA, 16–20 August 2016; pp. 586–589.
- Cao, L.; Tang, X.Q.; Wang, W.F. Tension optimization and experimental research of parallel mechanism driven by 8 cables for constant vector force output. *Robot* **2015**, *37*, 641–647.
- Wang, W.F.; Tang, X.Q.; Shao, Z.F. Design and analysis of a wire-driven parallel mechanism for large vertical storage tank. *J. Mech. Eng.* **2016**, *52*, 1–8.
- Zhang, B.; Shang, W.W.; Cong, S.; Li, Z. Coordinated dynamic control in the task space for redundantly actuated cable-driven parallel robots. *IEEE/ASME Trans. Mechatron.* **2020**, *26*, 2396–2407. [\[CrossRef\]](#)
- Ming, W.; Hornby, T.G.; Landry, J.M.; Roth, H.; Schmit, B.D. A cable-driven locomotor training system for restoration of gait in human SCI. *Gait Posture* **2011**, *33*, 256–260.
- Wang, Y.L.; Wang, K.-y.; Zhang, Z.-x.; Han, Z.; Wang, W.-l. Analysis of dynamical stability of rigid-flexible hybrid-driven lower limb rehabilitation robot. *J. Mech. Sci. Technol.* **2020**, *34*, 1735–1748. [\[CrossRef\]](#)
- Ennaïem, F.; Chaker, A.; Laribi, M.A.; Sandoval, J.; Bennour, S.; Mlika, A.; Romdhane, L.; Zeghloul, S. Task-Based Design Approach: Development of a Planar Cable-Driven Parallel Robot for Upper Limb Rehabilitation. *Appl. Sci.* **2021**, *11*, 5635. [\[CrossRef\]](#)
- Yang, Z.M.; Zi, B.; Chen, B. Mechanism Design and Kinematic Analysis of a Waist and Lower Limbs Cable-Driven Parallel Rehabilitation Robot. In Proceedings of the IEEE 3rd Advanced Information Management, Communicates, Electronic and Automation Control Conference, Chongqing, China, 11–13 October 2019; IEEE: Chongqing, China, 2019; pp. 723–727.
- Wang, Y.L.; Wang, K.Y.; Zhang, Z.X. Design, comprehensive evaluation, and experimental study of a cable-driven parallel robot for lower limb rehabilitation. *J. Braz. Soc. Mech. Sci. Eng.* **2020**, *42*, 1735–1748. [\[CrossRef\]](#)
- Rogério, S.G.; Carvalho, J.; Rodrigues, L.A.O.; Barbosa, A.M. Cable-Driven Parallel Manipulator for Lower Limb Rehabilitation. *Appl. Mech. Mater.* **2014**, *2828*, 535–542.
- Wang, K.-Y.; Yin, P.-C.; Yang, H.-P.; Tang, X.-Q. The man-machine motion planning of rigid-flexible hybrid lower limb. *Adv. Mech. Eng.* **2018**, *10*, 1687814018775865.
- Ghasem, A.; Jungwon, Y.; Hosu, L. Optimum kinematic design of a planar cable-driven parallel robot with wrench-closure gait trajectory. *Mech. Mach. Theory* **2016**, *99*, 1–18.
- Rosati, G.; Zanutto, D.; Agrawal, S.K. On the design of adaptive cable-driven systems. *J. Mech. Robot.* **2011**, *3*, 021004. [\[CrossRef\]](#)
- Nguyen, D.Q.; Gouttefarde, M. Study of Reconfigurable Suspended Cable-Driven Parallel Robots for Airplane Maintenance. In Proceedings of the 2014 IEEE/RSJ International Conference on Intelligent Robots and Systems, Chicago, IL, USA, 14–18 November 2014; pp. 14–18.

26. Gagliardini, L.; Caro, S.; Gouttefarde, M.; Girin, A. Discrete reconfiguration planning for cable-driven parallel robots. *Mech. Mach. Theory* **2016**, *100*, 313–337. [[CrossRef](#)]
27. Rosati, G.; Andreolli, M.; Biondi, A.; Gallina, P. Performance of cable suspended robots for upper limb rehabilitation. In Proceedings of the IEEE 10th International Conference on Rehabilitation Robotics (ICORR), Noordwijk, The Netherlands, 13–15 June 2007; pp. 13–15.
28. Mao, Y.; Agrawal, S.K. Design of a cable-driven arm exoskeleton (CAREX) for neural rehabilitation. *IEEE Trans. Robot.* **2012**, *28*, 922–931. [[CrossRef](#)]
29. Zanutto, D.; Rosati, G.; Minto, S.; Rossi, A. Sophia-3: A semiadaptive cable-driven rehabilitation device with a tilting working plane. *IEEE Trans. Robot.* **2014**, *30*, 974–979. [[CrossRef](#)]
30. Kim, H.; Miller, L.M.; Fedulow, I.; Simkins, M.; Abrams, G.M.; Byl, N.; Rosen, J. Kinematic data analysis for post-stroke patients following bilateral versus unilateral rehabilitation with an upper limb wearable robotic system. *IEEE Trans. Neural Syst. Rehabil. Eng.* **2013**, *21*, 153–164. [[CrossRef](#)] [[PubMed](#)]
31. Reza zadeh, S.; Behzadipour, S. Workspace analysis of multibody cable-driven mechanisms. *ASME J. Mech. Robot.* **2011**, *3*, 021005. [[CrossRef](#)]
32. Lau, D.; Oetomo, D.; Halgamuge, S.K. Generalized modeling of multilink cable-driven manipulators with arbitrary routing using the cable-routing matrix. *IEEE Trans. Robot.* **2013**, *5*, 1102–1113. [[CrossRef](#)]
33. Niku, S.B. *Introduction to Robotics: Analysis, Systems, Application*; Pearson Education: Upper Saddle River, NJ, USA, 2011.
34. Pan, H.J.; Ma, C.H.; Shen, S.F. Study on the maximum motion range of main joints of human limbs. *J. Zhejiang Norm. Univ. Nat. Sci. Ed.* **1995**, *3*, 64–68.
35. Strydom, M.L.; Banach, A.; Roberts, J.; Crawford, R.; Jaiprakash, A.T. Kinematic Model of the Human Leg Using DH Parameters. *IEEE Access* **2020**, *8*, 191737–191750. [[CrossRef](#)]
36. Jung, Y.; Bae, J. Kinematic Analysis of a 5-DOF Upper-Limb Exoskeleton with a Tilted and Vertically Translating Shoulder Joint. *IEEE/ASME Trans. Mechatron.* **2015**, *20*, 1428–1439. [[CrossRef](#)]
37. Khalipour, S.A.; Khorrambakht, R.; Taghirad, H.D.; Cardou, P. Robust cascade control of a deployable cable-driven robot. *Mech. Syst. Signal Process.* **2019**, *127*, 513–531. [[CrossRef](#)]
38. Santos, J.C.; Chemori, A.; Gouttefarde, M. Model predictive control of large-dimension cable-driven parallel robots. *Mech. Mach. Sci.* **2019**, *74*, 221–232.
39. Fang, S.; Cao, J.; Zhang, Z.; Zhang, Q.; Cheng, W. Study on High-Speed and Smooth Transfer of Robot Motion Trajectory Based on Modified S-shaped Acceleration/Deceleration Algorithm. *IEEE Access* **2020**, *8*, 199747–199758. [[CrossRef](#)]
40. Saravanan, R.; Ramabalan, S. Evolutionary Minimum Cost Trajectory Planning for Industrial Robots. *J. Intell. Robot. Syst.* **2008**, *52*, 45–77. [[CrossRef](#)]
41. Gasparetto, A.; Zanutto, V. A new method for smooth trajectory planning of robot manipulators. *Mech. Mach. Theory* **2007**, *42*, 455–471. [[CrossRef](#)]
42. Wang, H.F.; Zhu, S.Q.; Wu, W.X. INSGA-II based multi-objective trajectory planning for manipulators. *J. Zhejiang Univ. Eng. Sci.* **2012**, *46*, 622–628.